JOURNAL OF AIRCRAFT
Vol. 38, No. 6, November–December 2001

Assessing Computational Fluid Dynamics Predictions for Control Surface Effectiveness

Feng Jiang*
The Boeing Company, Long Beach, California 90807

This paper examines the capability of current computational fluid dynamics (CFD) methods to simulate results from a two-dimensional aileron effectiveness wind-tunnel test conducted with an aft-loaded airfoil with modest trailing-edge thickness to investigate Reynolds-number effects on aileron effectiveness characteristics. The results presented herein are follow on to a previous two-dimensional CFD simulation, which failed to capture measured Reynolds-number effects. As a result of this earlier study, the interaction of the airfoil flowfield with the tunnel sidewall viscous flow and sidewall suction used in the test is accounted for in this three-dimensional simulation. The three-dimensional predictions provide a substantially improved correlation with the experimental results. A very prominent aspect of the three-dimensional approach is the prediction of flow separation at the juncture of the airfoil and tunnel sidewall. This occurs in spite of the application of suction and raises serious doubts about the validity of scores of previous (and ongoing) CFD investigations, which have presumed that such two-dimensional airfoil test results were actually two-dimensional.

Nomenclature

C_l	=	lift coefficient
C_{l_0}	=	lift coefficient without aileron deflection
C_p	=	pressure coefficient
C_q	=	suction rate
M	=	corrected Mach number
Mo	=	corrected Mach number at zero aileron deflection
RN_C	=	Reynolds number based on chord
x/c	=	nondimensional chord station
y/c	=	nondimensional normal coordinate
α	=	angle of attack, deg
δ_a	=	angle of aileron deflection, deg

Introduction

THE need to extend state-of-the-art transonic computational fluid dynamics (CFD) capabilities to be able to reliably predict the aerodynamic effectiveness of trailing-edge control surfaces (ailerons, elevators, etc.) for a wide range of flight conditions is well established. This paper is a continuation of work reported previously.[1] The experimental data set used for this study is a rather unique set of ostensibly two-dimensional test results obtained with a representative aft-loaded airfoil configuration. A detailed account of the experimental setup and results, as well as the initial two-dimensional free-air CFD simulation results can be found in Ref. 1. Therefore, only a brief description will be included here.

The airfoil geometry used in this investigation is an aft-loaded "supercritical" type design, having a maximum thickness of 12.3% chord, a peak aft camber of 2.365% chord (located at 82% chord), and a trailing-edge thickness of 0.55% chord. The aileron hingeline is located at 75% chord. Boundary-layer control on the mostly solid sidewalls was provided via 18 × 24-in. porous suction panels which surround the 10-in.-chord/15-in.-span airfoil model. A suction rate C_q ranging from 0.007 to 0.0095 was employed during the test. A total of eight aileron deflections (−5, −2, −1, 1, 2, 3, 4, and 5 deg) were provided. Aerodynamic characteristics for this airfoil/aileron combination were measured over a range of angles of attack both with and without the aileron deflected in order to identify angle-of-attack, Mach-number, and Reynolds-number influences on aileron effectiveness. At a design cruise Mach number, data were obtained at chord Reynolds numbers of 5×10^6, 15×10^6, and 25×10^6 to define basic characteristics and Reynolds-number influences, thereby enabling quite detailed comparisons with CFD predictions, and a good understanding of the prevailing flow physics. This data set provides some good test cases with a separation problem evident near the trailing edge when the aileron is deflected at low Reynolds numbers at modest airfoil incidence angles that either goes away at higher Reynolds numbers or is greatly reduced in size. Then, at the 15×10^6, data were obtained at a higher Mach number to help define and better understand some very sizable reductions in aileron effectiveness, which occur with increasing freestream Mach number.

For trailing-edge-up aileron deflections the effectiveness is quite linear. In contrast, with trailing-edge-down aileron deflections the effectiveness departs from the linear trend. The cause for this loss of aileron effectiveness appears to be mainly caused by the trailing-edge-type separation on the upper surface. Measured results indicate that there is generally a "favorable" (i.e., improving with increasing) Reynolds-number effect on aileron effectiveness. Reductions in the trailing-edge-down aileron effectiveness characteristics at the higher Mach number are also obvious in the test data, which are mostly associated with a very limited aft movement of the upper-surface shock as the aileron is deflected. This, in turn, is certainly related to the magnitude of flow separation over the aileron.

Some success was realized previously in duplicating the subject two-dimensional measured aileron effectiveness characteristics with a two-dimensional free-air CFD approach.[1] Relatively good agreement between the measured and CFD-predicted aileron effectiveness characteristics was obtained in a number of cases, particularly at the higher Reynolds numbers, higher Mach numbers, and/or higher angles of attack. However, at the lower Reynolds number of 5×10^6 two-dimensional CFD results overpredicted the aileron effectiveness, thereby failing to capture a very noticeable reduction in aileron effectiveness seen experimentally. Related to this overprediction is the disconnect between the measured and CFD-predicted shock locations, starting with the undeflected-aileron baseline. It indicates an erroneous freestream Mach number, which causes suspicion that the experimental database may well not be just a two-dimensional flow. A three-dimensional CFD simulation that includes the tunnel sidewalls is necessary in order to capture a really three-dimensional flowfield.

Received 1 February 2000; revision received 9 July 2001; accepted for publication 12 August 2001.

*Senior Engineer/Scientist, Flight Technology Group, MC C078-0532, 2410 E. Wardlow Road.

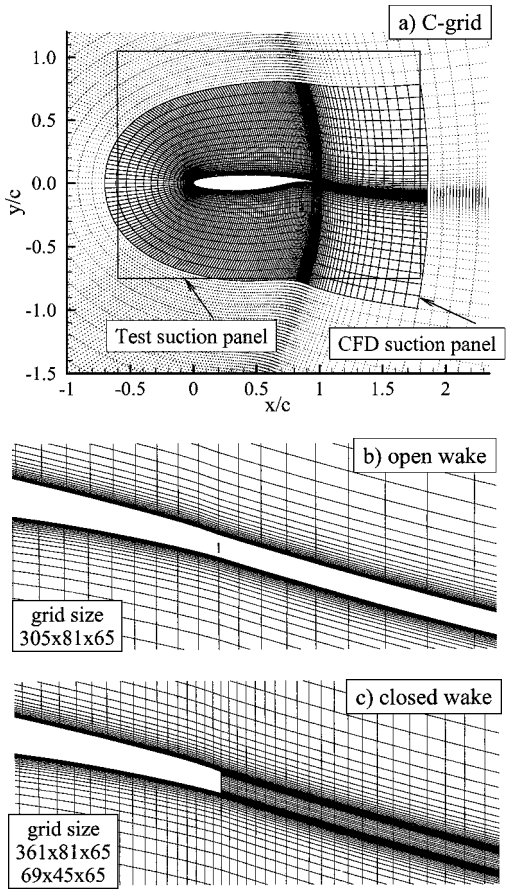

Fig. 1 Grid topologies.

Three-Dimensional CFD vs Experimental Results

Background

The flow solver CFL3D (version 5) was employed in this study. It has the Spalart–Allmaras (one-equation) turbulence model incorporated. At the start of this CFD assessment study, a single-zone C-grid topology (as illustrated in Fig. 1a) was used in conjunction with an open-wake modeling approach (see Fig. 1b). A one-to-one block interface boundary condition is used for the wake region. This "open-wake" approach was adopted at the start of this study based on results of previous studies of three-dimensional wings with thick trailing edges where CFD-predicted pressures obtained this way closely matched corresponding experimental results in the trailing-edge region. Computational requirements are also noticeably less with this approach. Later on when some of the anomalies between CFD predictions and test results emerged, particularly when flow separation was involved, it was suggested that perhaps a closed-wake modeling approach would be more appropriate. The closed-wake modeling subsequently implemented, as illustrated in Fig. 1c, utilizes the addition of a wake block together with a localized increase in (chordwise) grid density. Transition locations on both the upper and lower surface of the airfoil for the CFD predictions were specified to match either where transition was tripped in the test, or where it was known to occur in the test. At 5×10^6 Reynolds-number, transition was specified at 15 and 28% chord for the upper and lower surface respectively. At 15×10^6 Reynolds number, the locations were at 10 and 15% chord respectively, and then, at 25×10^6, transition was specified at the leading edge.

Two methods of incorporating the three-dimensional effects of the tunnel walls (floor, ceiling, and sidewalls) in the computational analysis/modeling of the subject test setup were considered. Specific modeling of the sidewall viscous characteristics, including the presence of the sidewall suction system used in the experiment to provide a healthier sidewall boundary layer around the model less prone to separation, was an essential part of both because of the perceived importance of these effects. The difference between the two methods was in how the effects of the porous floor and ceiling were to be accounted for. The two options considered for incorporating these effects involved either specifically modeling these (porous) surfaces in the CFD analysis or applying the standard Mokry corrections[2] and ending up with a three-dimensional free-air assessment. The latter option was selected because there is a very strong belief that three-dimensional effects caused by the sidewall viscous characteristics right around the airfoil model are much, much greater than any three-dimensional effects imposed on the model by the more remote tunnel floor and ceiling. Also, knowing that the computational modeling of the (more important) sidewall influence was an approximation, taking into account some of the likely limitations of the turbulence models being employed for some of the flow situation involved, and considering some of the uncertainties involved in deciding just how to best model the airfoil trailing-edge thickness, further refining the influence of the (more remote) porous floor and ceiling did not seem to be prudent (which would also involve an approximation).

Specifics as to how to model the sidewall boundary layer, including the suction panel that surrounds the model, were guided by previous studies,[3,4] which examined how to match empty tunnel sidewall boundary-layer thickness at the model location vs Reynolds number and suction level. For the results shown in this study, the turbulent boundary layer was assumed to originate at $x/c = -14$, and suction rates were specified to match corresponding experimental measurements. At the nominal Mach number suction rates of -0.007, -0.0085, and -0.0095 were used at 5×10^6, 15×10^6, and 25×10^6 Reynolds numbers, respectively. A suction rate of -0.008 was used at the higher Mach-number condition at 15×10^6 Reynolds number. Although these variations, i.e., increasing with increasing Reynolds number, and decreasing with increasing Mach number, are the opposite of what would normally be desired, these suction rates are largely dictated by the static pressure level in the test section at these conditions.

Most of the CFL3D computations for this three-dimensional free-air assessment were obtained using the Spalart–Allmaras (S–A) turbulence model. However, a few cases were studied using the Mentor's shear stress transport (SST) model, and Wilcox's k–ω model. As will be seen, the basic airfoil characteristics obtained using the Wilcox k–ω model deviated from the experimental results noticeably more than others, and as a consequence it was quickly dropped from further consideration. Mentor's SST model was, however, used more extensively. Even though the results obtained using it were, as was the case in the previous two-dimensional study (Ref. 1.), very similar to those obtained with the S–A model, it did have the advantage of having slightly better convergence characteristics for cases involving significant flow separation at the model/sidewall juncture.

Basic Airfoil Characteristics

Because predictions and/or measurements of aileron effectiveness characteristics are typically cast in terms of increments or changes relative to the aerodynamic characteristics of the basic airfoil/wing with undeflected ailerons, the ability to accurately/adequately predict these baseline characteristics is clearly a prerequisite for successfully predicting the characteristics with the aileron deflected. Comparisons of the three-dimensional CFD predictions using open-wake modeling and the corresponding experimental lift curves for 5×10^6, 15×10^6, and 25×10^6 Reynolds numbers at the nominal cruise Mach number are presented in Fig. 2. It can be seen that the correlation is superb at 25×10^6 Reynolds number, still very well at 15×10^6, and not that bad at 5×10^6. Some notable results include the noticeably poorer correlation obtained at 5×10^6 Reynolds number with the Wilcox k–ω model and the very close agreement seen between predictions obtained using the S–A and SST turbulence models.

An assessment of the relative advantages and disadvantages of open- vs closed-wake modeling of the thick trailing edge was also done as part of this three-dimensional free-air study of the basic airfoil characteristics. At the nominal cruise Mach-number condition closed-wake predictions using the S–A model were made at both 5×10^6 and 15×10^6 Reynolds numbers for comparison with the corresponding open-wake predictions. In addition, a couple of cases were also studied at 5×10^6 using the Mentor's SST model.

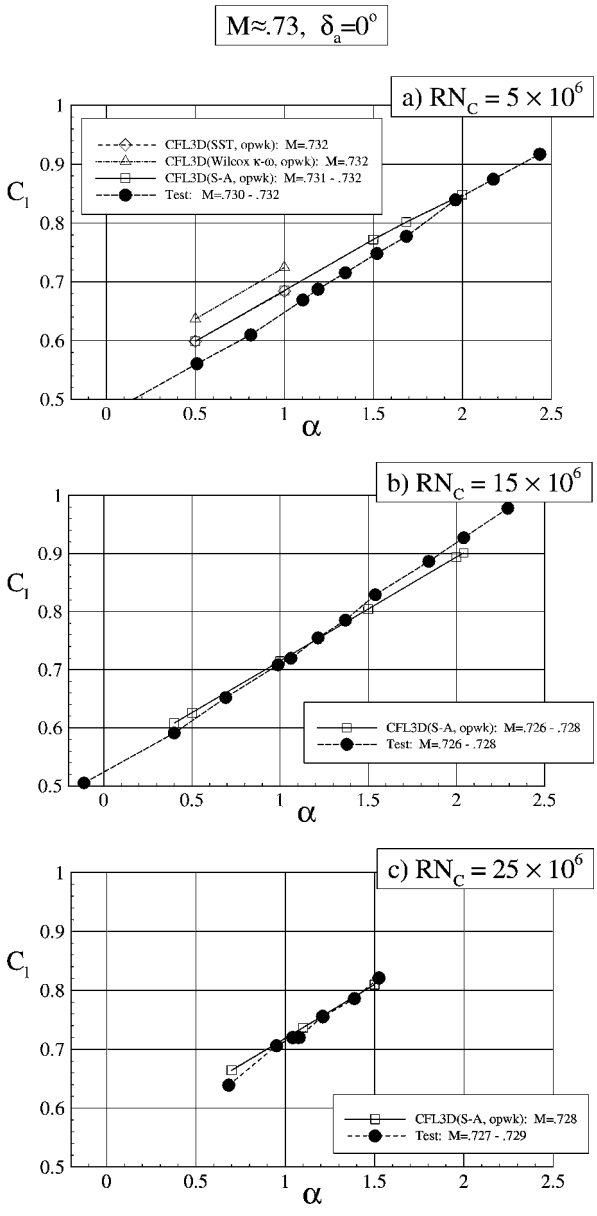

Fig. 2 Comparisons of Reynolds-number effects on baseline lift characteristics predicted by CFL3D with the test data at 0.73 Mach number.

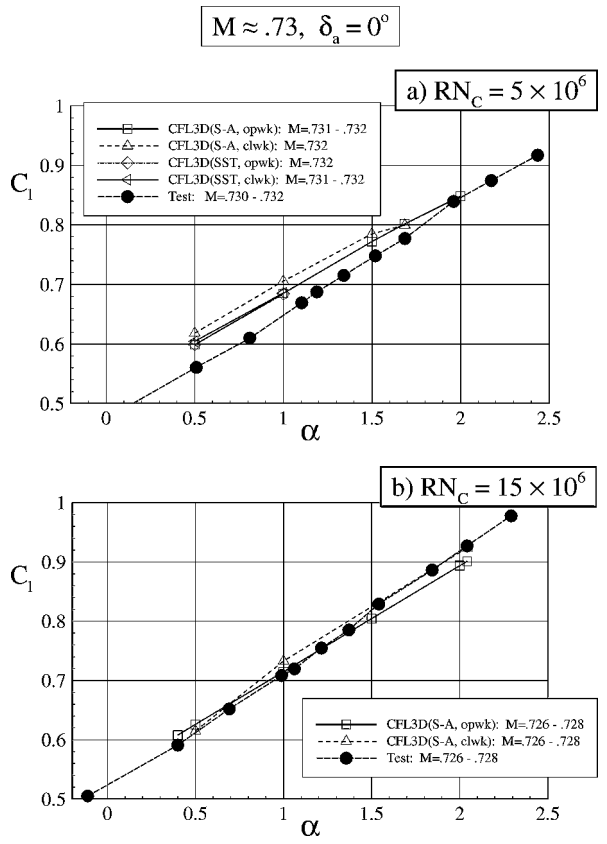

Fig. 3 Comparisons of lift characteristics between the test data and CFD predictions with different wake grid topologies at Mach = 0.73, δ_a = 0 deg.

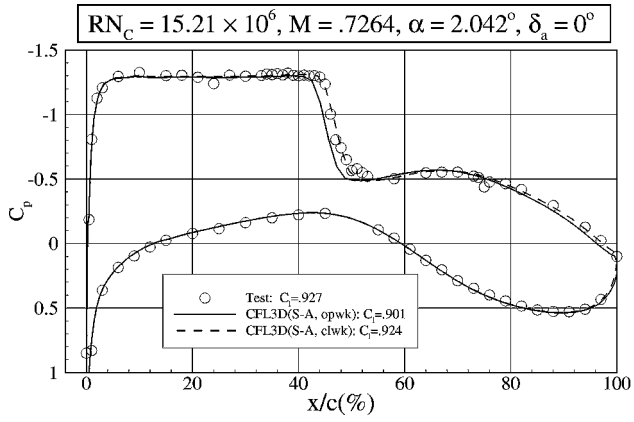

Fig. 4 Comparisons of pressure distributions predicted by CFL3D (S–A) at $RN_C = 15 \times 10^6$ with different wake grids.

The resulting comparisons are shown in Fig. 3. As can be seen, at 5×10^6 Reynolds number the closed-wake predictions obtained using the S–A model produce a slightly higher lift than predicted with the open-wake assessment, resulting in a slightly poorer correlation with the experimental results. A different trend is seen in the comparisons obtained using Mentor's SST model. There is essentially no difference between the open- and closed-wake predictions (at least for the two angles of attack addressed). Contrary to the trend seen at 5×10^6, at 15×10^6 Reynolds number using the S–A model, the closed-wake predictions provide an improved correlation with the test results. The improvement is most apparent at the higher angles of attack, as shown in Fig. 3b, which results in a better prediction of the lift-curve slope.

The predicted airfoil (centerline) pressure distributions at 15×10^6 Reynolds number and angle of attack of $\alpha = 2.04$ deg are shown in Fig. 4. By comparing these results with the corresponding two-dimensional free-air predictions (see Fig. 13 in Ref. 1), a few improvements are apparent. Most obvious is the excellent duplication of the measured upper-surface rooftop shape/level and shock location achieved with the three-dimensional analysis. It can also be seen that the improved correlation achieved with the closed-wake modeling at this condition is, in addition, a direct consequence of a more accurate prediction of the shock location and aft-upper-surface pressure level. The resulting correlation achieved in this case is so good that the closed-wake CFD predictions have the appearance of being a fairing through the test results.

A corresponding comparison at 5×10^6 Reynolds number is shown in Fig. 5, where it can be seen that the correlation is not quite as good as at 15×10^6. The overprediction of the lift seen in Fig. 3a is caused by a combination of a slight overprediction of the rooftop suction pressure levels ahead of the shock, a predicted shock location which is slightly too far aft, and a small overprediction of the lower-surface contribution to the aft loading. Although the aft-upper-surface pressure level is again more accurately predicted with the closed-wake modeling, this improvement is largely offset by a predicted aft movement of the shock, placing it even further aft of the experimental results. A potential cause for much of the relatively poorer correlation obtained at 5×10^6 Reynolds number is a less representative prediction of the flow separation characteristics

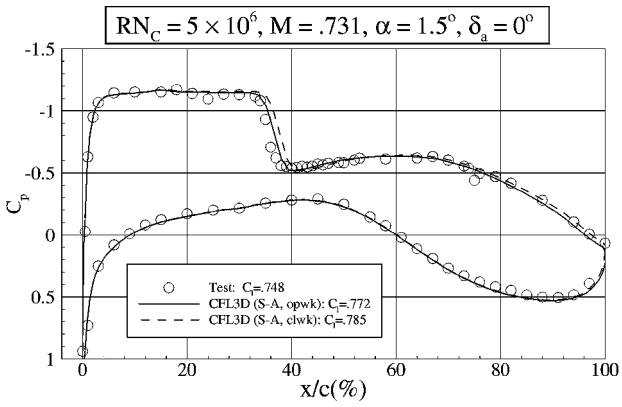

Fig. 5 Comparisons of pressure distributions predicted by CFL3D (S–A) at $RN_C = 5 \times 10^6$ with different wake grids.

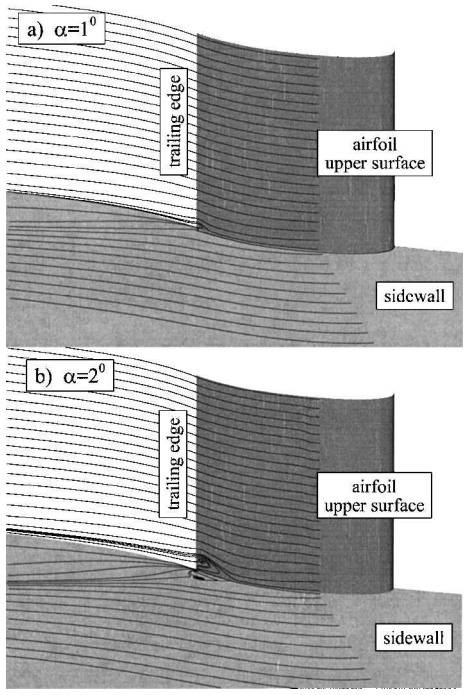

Fig. 6 Particle traces on airfoil upper surface for $RN_C = 5 \times 10^6$, Mach = 0.73, $C_q = -0.007$, $\delta_a = 0$ deg.

existing in the model/sidewall juncture region. Such an occurrence would not come as a big surprise, however, because predictions of initial separation onset/progression characteristics remains as perhaps the largest challenge for modern CFD (i.e., Reynolds-averaged Navier–Stokes), and this is probably particularly true for juncture flows.

To permit some understanding of the magnitude of the (predicted) juncture flow separations involved in the foregoing cases, particle traces on the airfoil upper surface and tunnel/sidewall have been examined at both 5×10^6 and 15×10^6 Reynolds numbers and $\alpha = 1$ and 2 deg. The particle traces for 5×10^6 Reynolds number cases are illustrated in Fig. 6. Apparent from these predictions is the existence of juncture-flow separation at both conditions, with a pronounced growth in the size of the predicted separation region as the angle of attack is increased.

The corresponding predictions for 15×10^6 Reynolds number are displayed in Fig. 7, which indicates that increasing Reynolds number (and sidewall suction rate) does reduce the size of the (predicted) separated flow regions as anticipated. Although there is a legitimate concern regarding the accuracy of these juncture-flow-separation predictions, the excellent correlation seen previously in Fig. 4 at 15×10^6 Reynolds number does strongly suggest that the

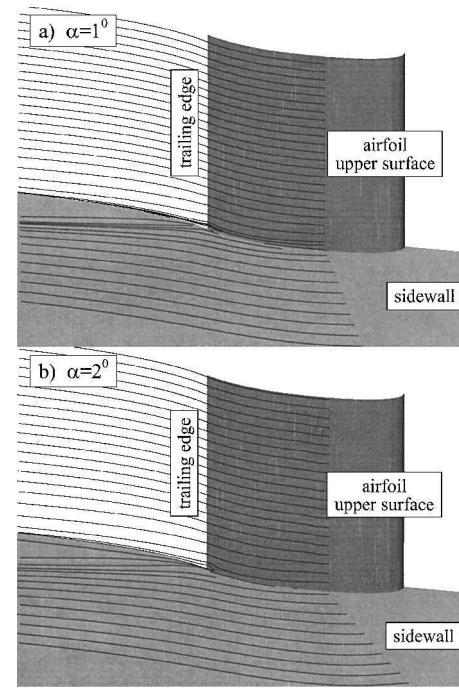

Fig. 7 Particle traces on airfoil upper surface for $RN_C = 15 \times 10^6$, Mach = 0.73, $C_q = -0.0085$, $\delta_a = 0$ deg.

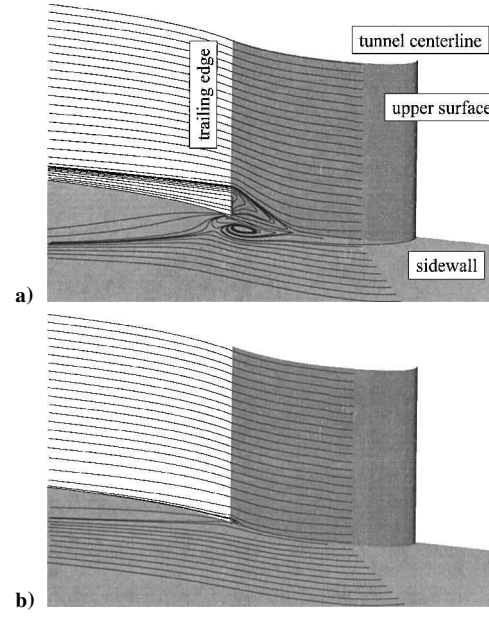

Fig. 8 Particle traces on the airfoil upper surface at $RN_C = 15.21 \times 10^6$, Mach = 0.7264, $\alpha = 2.042$ deg, and $\delta_a = 0$ deg: a) without suction and b) with suction.

predictions at $RN_C = 15 \times 10^6$ shown in Fig. 7 are, most likely, reasonably representative.

The importance of having had sidewall-boundary-layer suction capability available and operating during this test program cannot be overstated, even though the maximum suction rates possible (at least at 5×10^6 and 15×10^6 Reynolds numbers) are not sufficient to eliminate (predicted) juncture-flow separation for some of the test conditions. A good indication of the effectiveness and importance of having sidewall suction can be seen by comparing predicted particle traces at the suction rate employed during the testing with those predicted without any suction. One such comparison at 15×10^6 Reynolds number and $\alpha = 2.04$ deg is shown in Fig. 8. Even though the suction rate possible (i.e., -0.0085) at this Reynolds number is indicated to be not quite adequate to completely eliminate the

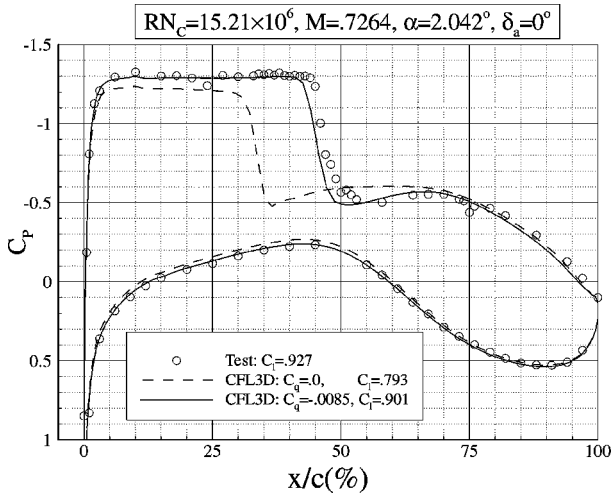

Fig. 9 Pressure distributions predicted by CFL3D (S–A) with and without suction; C_q is the suction rate.

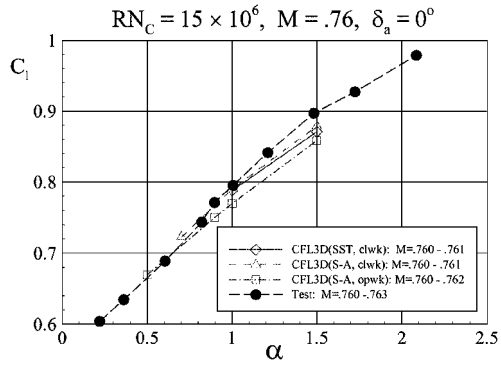

Fig. 10 Comparisons of lift characteristics predicted by CFL3D with the test data at higher Mach number.

juncture-flow separation, it does provide a very large reduction in the size of separated flow region, which would have existed without suction. As clearly indicated by the pressure distribution comparisons in Fig. 9, results obtained without any sidewall suction would be neither representative nor very meaningful.

A similar trend is observed for 5×10^6 Reynolds number cases. There is, however, one important difference, and that is in the size of the predicted juncture-flow separations at the experimental sidewall suction rates. The predicted separation area is noticeably larger at the lower Reynolds number. Although some portion of this difference is caused by the reduced suction rate available at the lower Reynolds number, it is not the major cause for the difference. Most of it appears to be a predicted Reynolds-number effect, but just how accurate this predicted difference is remains the issue. Qualitatively, it is probably appropriate. Unfortunately, the accuracy of the ensuing three-dimensional predictions of Reynolds number and angle-of-attack influences on control surface effectiveness will be strongly dependent upon the accuracy of these juncture-flow separation predictions on the baseline configuration, as well as the accuracy of such predictions when the aileron is deflected. This is not a comforting thought. Neither is the prospect that many analyses of so-called two-dimensional test results carried out in the past were likely misguided because of unaccounted-for sidewall and juncture-flow viscous effects, independent of whether sidewall suction was used or not in the experiments.

Similar improvements in the comparison of CFD predictions with the test results for the baseline airfoil were also obtained with the three-dimensional predictions at the higher-Mach-number condition (at 15×10^6 Reynolds number), but the same concerns regarding the accuracy of juncture-flow separation predictions are definitely present in this case as well, particularly at higher angles of attack. The comparison of the predicted lift curves with the test results at this condition is shown in Fig. 10. The predictions at $\alpha = 1.5$ deg start to

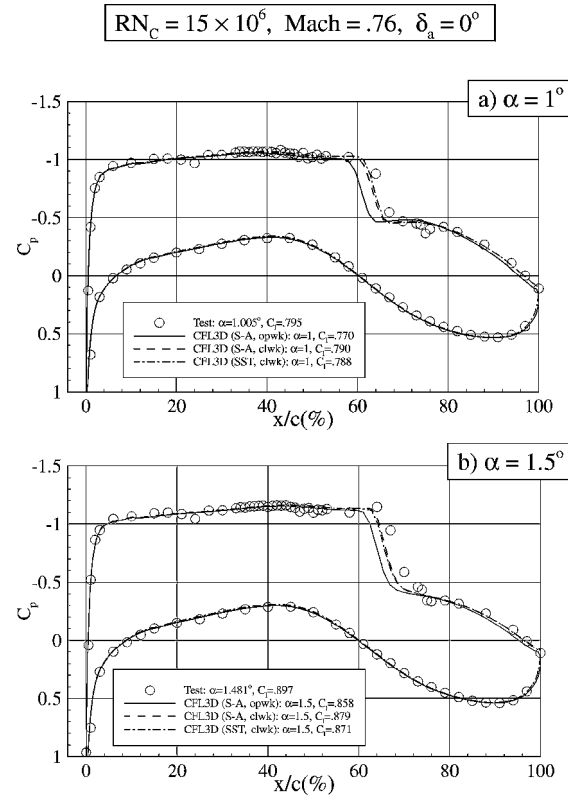

Fig. 11 Comparisons of pressure distributions predicted by CFL3D with different wake grid topologies for $RN_C = 15 \times 10^6$, Mach = 0.76, $\delta_a = 0$ deg.

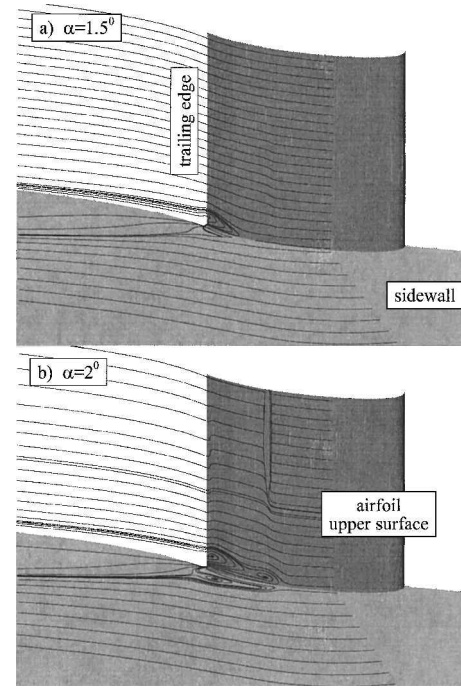

Fig. 12 Particle traces on airfoil upper surface for $RN_C = 15 \times 10^6$, Mach = 0.76, $\delta_a = 0$ deg.

show the earlier roundover. Examining the predicted and measured pressure distributions shown in Fig. 11 at $\alpha = 1$ and 1.5 deg can identify the source of this earlier roundover. The predicted shock locations are noticeably further forward of the measured location. Convergence difficulties prevented obtaining any adequately converged CFD solutions at angles of attack above 1.5 deg.

Predicted particle traces for this higher-Mach-number test condition are shown in Fig. 12, and the partially-converged solution

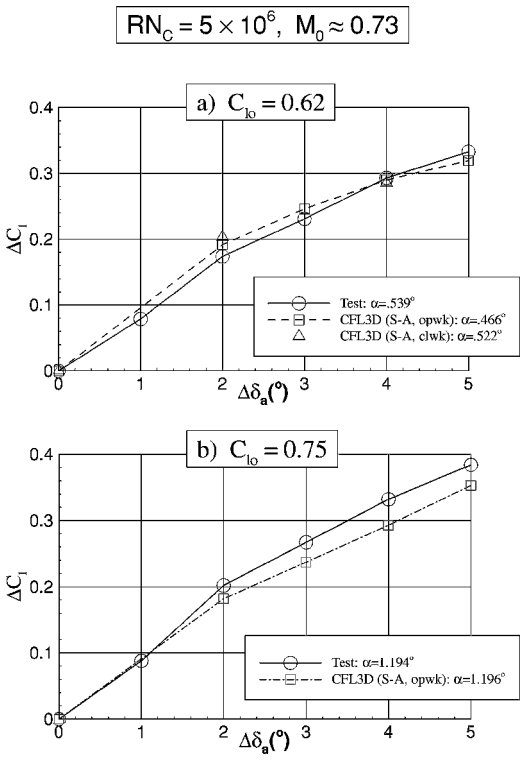

Fig. 13 Aileron effectiveness—three-dimensional free-air CFD vs measured at $RN_C = 15 \times 10^6$, $M_0 \approx 0.73$.

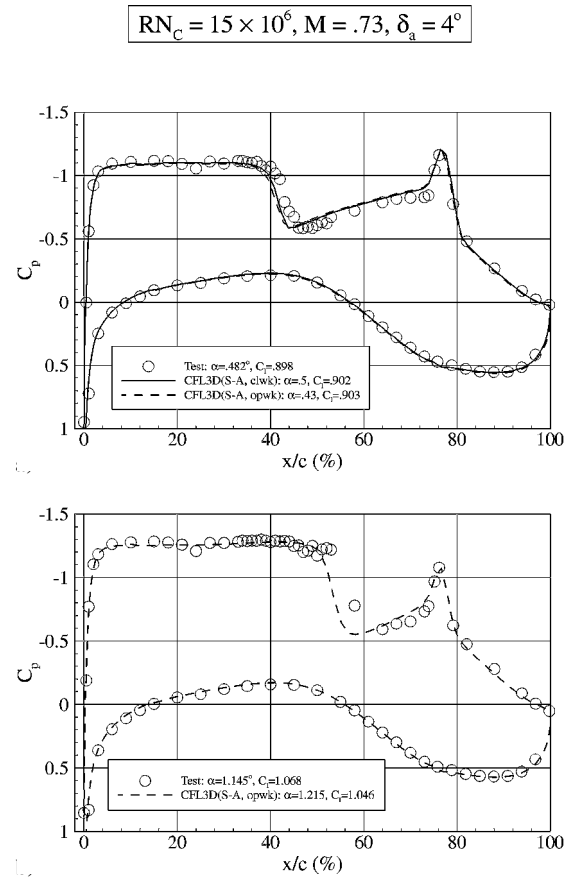

Fig. 14 Comparisons of C_p distributions between CFD predictions and test data at $RN_C = 15 \times 10^6$, $M = 0.73$, $\delta_a = 4$ deg: a) $C_{lo} = 0.61$ and b) $C_{lo} = 0.75$.

obtained at $\alpha = 2$ deg (with Mentor's SST model) indicates a very dramatic increase in the size of the juncture-flow separation as the angle of attack is increased from 1.5 to 2 deg. This behavior likely explains the convergence difficulties encountered. Again, this predicted trend (from 1.5 to 2 deg) is likely qualitatively appropriate, but the magnitude of the change indicated may not be representative.

Aileron Effectiveness Characteristics

Comparisons of CFD-predicted and measured aileron effectiveness characteristics in this section are performed in each case at their respective angle of attack for consistent/selected undeflected-aileron lift levels. This is necessary in order to provide meaningful comparisons because of the offset between the CFD-predicted and measured lift curves for the undeflected-aileron reference case (see Fig. 2). The predicted trailing-edge-down aileron effectiveness characteristics for the nominal cruise Mach number at 15×10^6 Reynolds number for the low and intermediate lift levels are summarized in Fig. 13 and compared with the corresponding experimental results. At the lower lift level where sidewall juncture-flow separation has a reduced impact, the predictions are in excellent agreement with the experimental results, and there is little difference between the open- and closed-wake predictions. However, at the intermediate lift level where sidewall juncture-flow separation is more of an issue the aileron effectiveness is underpredicted.

Understanding of the reasons behind the excellent agreement between the test results and the CFD predictions at the lower lift level, as well as the underprediction of the aileron effectiveness at the intermediate lift level, can be gained by examining the comparisons of the predicted- and measured-pressure distributions shown in Fig. 14 for aileron deflections of 4 deg. At the lower lift level the predicted shock location is slightly forward of the measured location, but the resulting underprediction of the lift is offset by a small overprediction of the suction pressure level aft of the shock. On the other hand, at the intermediate lift level the shock location discrepancy is a bit larger, and there is less of an offset from the overprediction of the suction pressures aft of the shock, resulting in the noticeable underprediction of the aileron effectiveness at this condition. It is also of significance to note the excellent agreement between the measured and predicted upper-surface pressure distributions near the trailing edge seen in Fig. 14. This is in contrast to the premature (or excessive) prediction of flow separation approaching the trailing edge seen previously with the two-dimensional free-air predictions[1] at the intermediate lift level, thereby clearly illustrating that there is likely some three-dimensional relief provided by the juncture-flow separation in the CFD predictions (at the model centerline). Some of this three-dimensional relief can also be brought about by a more-forward-predicted shock location in the three-dimensional predictions, where the predicted shock location is slightly forward of the measured location rather than further aft as was the case with the two-dimensional predictions at this condition.

Turning next to the CFD predictions of aileron effectiveness characteristics at the 5×10^6 Reynolds number and nominal cruise Mach-number condition, comparisons of the predicted and measured aileron effectiveness characteristics are illustrated in Fig. 15. The correlation between predicted and measured characteristics is quite good. At the lower lift level, where closed-wake solutions are also obtained, the open- and closed-wake predictions tend to straddle the experimental results. A couple of interesting observations regarding these low-Reynolds-number predictions can be made by examining the comparisons of measured and CFD-predicted pressure distributions shown in Fig. 16. At the lower lift level the comparison with the open-wake modeling is clearly better than that with the closed-wake modeling approach. These results indicate that the reasonably close (integrated) prediction of the measured aileron effectiveness characteristics obtained with the closed-wake modeling approach can well be a bit more fortuitous than the similar agreement obtained with the open-wake modeling approach. However, the big question mark in all this is just how good (or bad) are the predicted juncture-flow separation characteristics. The second, and perhaps more important observation, is the disconnect seen between the predicted and measured indications of the extent of upper-surface flow separation approaching the trailing edge as the ailerons are deflected trailing edge down. It can be seen in Fig. 16 at both lift

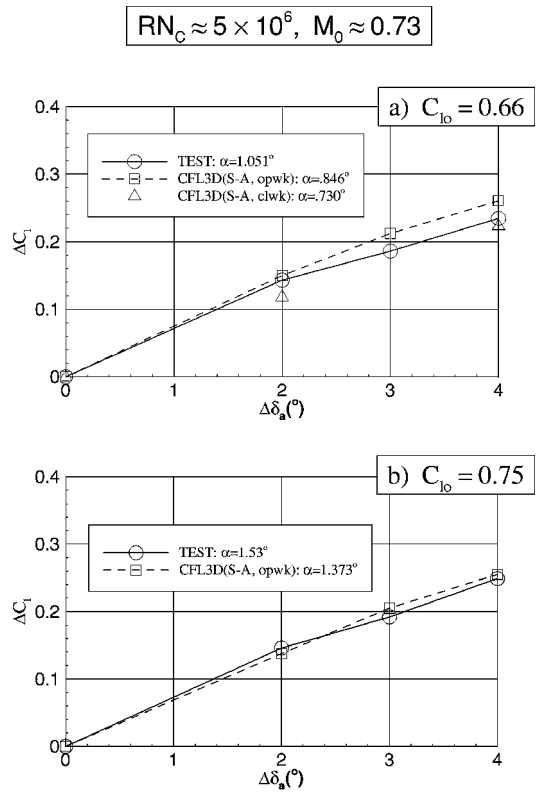

Fig. 15 Aileron effectiveness—three-dimensional free-air CFD predictions vs measured at $RN_C = 5 \times 10^6$ and $M_0 \approx 0.73$.

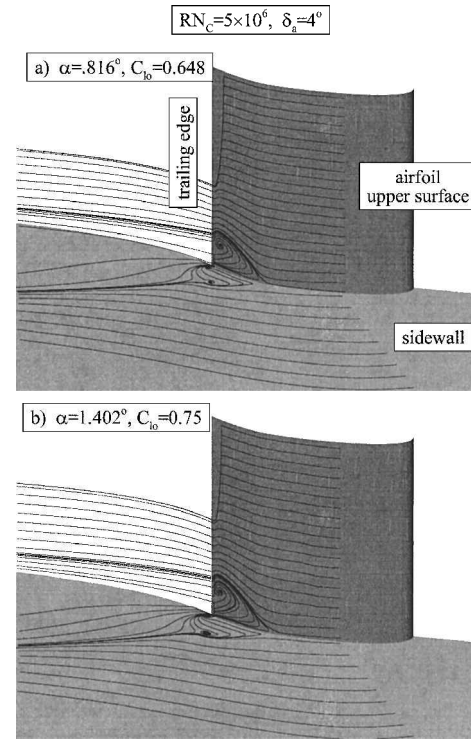

Fig. 17 Particle traces on the airfoil upper surface at $RN_C = 5 \times 10^6$, $M = 0.73$, $C_q = -0.007$, $\delta_a = 4$ deg.

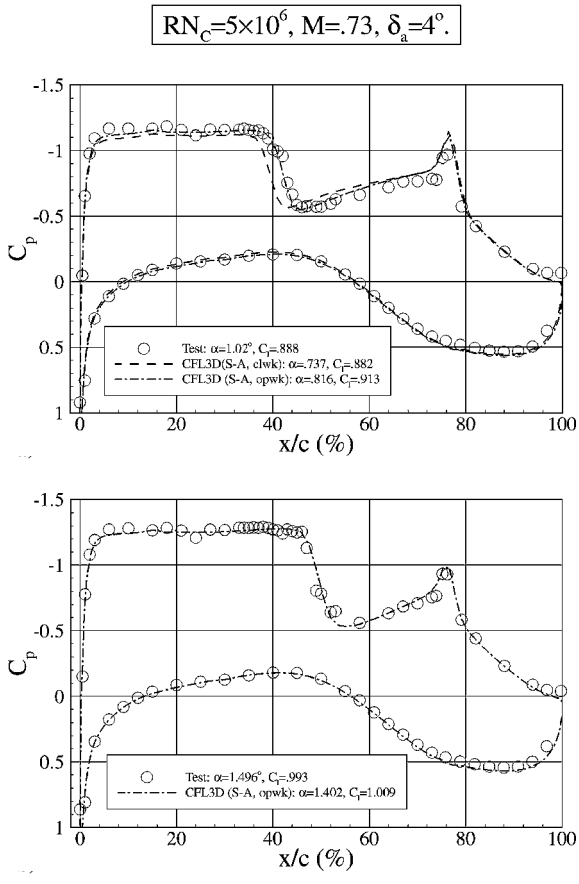

Fig. 16 Comparisons of C_p distributions between CFD predictions and test data at $RN_C = 5 \times 10^6$, $M = 0.73$, $\delta_a = 4$ deg: a) $C_{lo} = 0.648$ and b) $C_{lo} = 0.75$.

conditions that the predicted flow deterioration (i.e., separation) in this area is definitely not as adverse as the measured results indicated. Although the failure in this case to predict the extent of the trailing-edge separation may well not have a real large impact on the aileron effectiveness level, experience (i.e., DC-10, etc.) has shown that such separations can, in some cases, lead to quite major reductions in aileron effectiveness.[5] Hence, the present inability to accurately predict the onset/progression of such separations is a major limitation. However, in all fairness it should be recognized that this particular set of experimental results is a real tough test case because of the presence/influence of sidewall juncture-flow separation. And, there is not a high degree of confidence in the absolute accuracy of the present predictions of this juncture-flow region, especially predicted Reynolds-number effects. But, as already indicated, the predicted trends are representative.

With regard to the predicted juncture-flow separations, predicted particle traces for a trailing-edge-down aileron deflection of 4 deg at both the lower and intermediate lift level at this lower Reynolds number are provided in Fig. 17. Predicted trends are very similar to those at 15×10^6 Reynolds number, i.e., the size of the juncture-flow separation increases a bit as the lift level is increased, while the size of the trailing-edge separated region at the centerline shrinks a little. However, at this Reynolds number even though the trends appear to be consistent with the experimental results the magnitude of the centerline flow separation is not. How much of this disconnect is attributable to fundamental turbulence modeling limitations, or how much is attributable to an inaccurate prediction of the juncture-flow separation, remains an open question. Lastly, the comparisons of the measured and CFD-predicted variations in aileron effectiveness with changes in Reynolds number are examined. These comparisons, for both 2- and 4-deg trailing-edge-down aileron deflections at the two lift levels, are shown in Fig. 18. For the smaller deflection angle it can be seen that the reduction in aileron effectiveness observed experimentally as the Reynolds number is decreased from 15×10^6 to 5×10^6 is captured very well by the three-dimensional predictions. But, at the higher deflection angle only about half of the measured reduction is captured. However, this is a significant improvement over the two-dimensional free-air predictions,[1] where less than one-fourth of the reduction was captured. Hence, it is quite

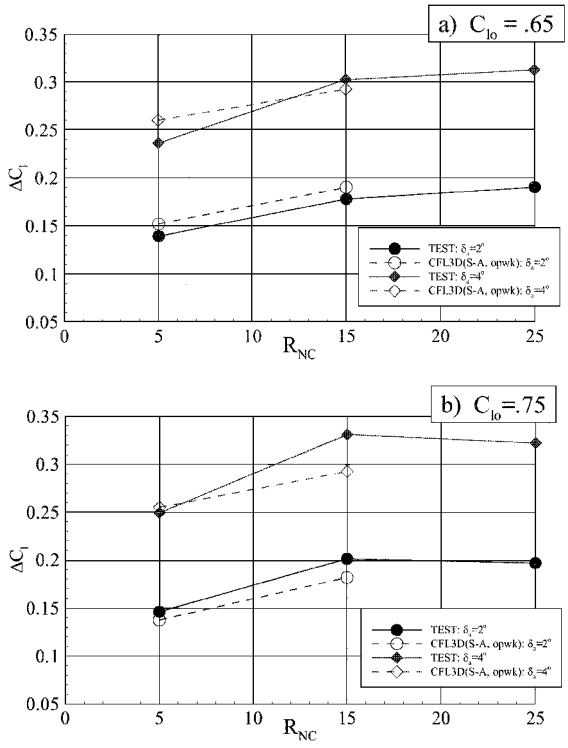

Fig. 18 Reynolds-number effects on aileron effectiveness—three-dimensional CFD predictions vs measured at $M_0 \approx 0.728$.

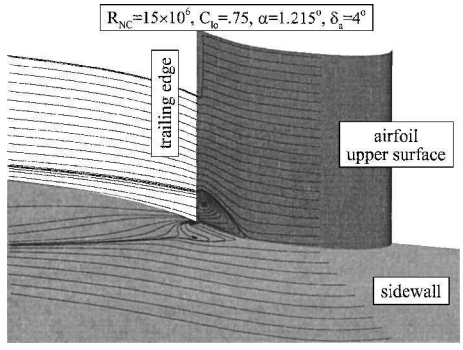

Fig. 19 Particle traces on the airfoil upper surface at $RN_C = 15 \times 10^6$, $M = 0.73$, $\delta_a = 4$ deg.

clear that (at least) a significant part of the Reynolds-number effects observed in this test program were attributable to tunnel sidewall viscous effects/interactions.

With regard to the inability to predict more of the experimentally observed Reynolds-number effect at the larger aileron deflection angle, it would not be at all surprising if inaccuracies in the predicted Reynolds-number effect of the sidewall juncture-flow separation were the major culprit. Although, as can be seen by comparing the particle traces at 15×10^6 Reynolds number shown in Fig. 19 with the corresponding one at 5×10^6 Reynolds number in Fig. 17b, the predicted region of juncture-flow separation is clearly smaller at $RN_C = 15 \times 10^6$ than it is at $RN_C = 5 \times 10^6$, it remains a question whether this predicted difference is either correct, too large, or too small.

Conclusions

Experimental data from a wind-tunnel test of a two-dimensional airfoil with deflectable trailing-edge aileron covering a fairly wide range of Reynolds numbers have been used to assess/calibrate the capabilities of the current state-of-the-art Reynolds-averaged Navier–Stokes methods for predicting aileron effectiveness characteristics. Conclusions reached as a consequence of this study are as follows:

1) Although the airfoil model was two-dimensional, the resulting flow around the airfoil in this ostensibly two-dimensional test turned out to have some very significant three-dimensional features arising from the viscous flow on the tunnel sidewall. This is believed to be a widespread malady with most purported two-dimensional airfoil tests.

2) Complete three-dimensional CFD modeling using the Spalart–Allmaras turbulence model, including the viscous flow on the tunnel sidewall (with suction applied), provided a much better match with the experimental measurements than the two-dimensional CFD modeling in general, but some specific accuracy issues/questions still remain unresolved.

3) Considering the strong three-dimensional viscous effects present with these experimental results, centered on very-hard-to-reliably-predict flow separation in the model-to-tunnel sidewall juncture region, these results turned out to represent a very (overly) complex test case rather than the relatively simple one intended.

4) The 0.55%-chord-thick trailing-edge geometry of the airfoil used in this study led to some options regarding how to best model it in the CFD studies. Both closed- and open-wake modeling concepts were used. The closed-wake approach does appear to provide a better representation of the flow physics, but it does carry the burden of increased computational time and poorer convergence characteristics. However, even though the closed-wake approach appears to be a better approach it still has some shortcomings. Consequently, it would not be realistic to believe that CFD with known turbulence models can accurately predict the drag of such thick-trailing-edge geometries.

Acknowledgments

This study was carried out under the auspices of the Integrated Wing Design Program, an element of the NASA Advanced Subsonic Technology Program. The author would like to thank Frank T. Lynch, program and technical manager, Integrated Wing Design, Boeing, Long Beach, California, for his continuous guidance and his technical and editorial contributions to this paper. She is also grateful to Y. Y. Chan (Institute for Aerospace Research, Canada), Mark Potsdam, and Arvin Shmilovich for their most helpful contributions during this study.

References

[1]Jiang, F., "CFD Modeling of 2-D Aileron Effectiveness," Society of Automotive Engineers, Paper 1999-01-5618, Oct. 1999.

[2]Mokry, M., "Subsonic Wall Interference Corrections for Finite-Length Test Sections Using Boundary Pressure Measurements," *Wall Interference in Wind Tunnels*, Paper 10, AGARD-CP-335, Sept. 1982.

[3]Ohmen, L. H., Brown, D., Chan, Y. Y., Galway, R. D., Hashim, S. M., Khalid, M., Malek, A., Mokry, M., Tang, N., and Thain, J., "New Transonic Test Sections for the NAE 5ft × 5ft Trisonic Wind Tunnel," National Academy of Engineering, Paper AN-62, Jan. 1990.

[4]Chan, Y. Y., "Boundary Layer Controls on the Sidewalls of Wind Tunnels for Two-Dimensional Tests," *Journal of Aircraft*, Vol. 17, No. 5, 1980, pp. 380–382.

[5]Lynch, F. T., "Commercial Transports—Aerodynamic Design for Cruise Performance Efficiency," *Transonic Aerodynamics*, edited by David Nixon, Vol. 81, Progress in Astronautics and Aeronautics, AIAA, New York, 1982, pp. 81–147.